Acta Materialia 96 (2015) 292–300

Contents lists available at ScienceDirect

Acta Materialia

journal homepage: www.elsevier.com/locate/actamat

Elastocaloric effect in $Ni_{50}Fe_{19}Ga_{27}Co_4$ single crystals

Fei Xiao [a], Mingjiang Jin [a], Jian Liu [b,c,*], Xuejun Jin [a,*]

[a] State Key Lab of Metal Matrix Composite, School of Materials Science and Engineering, Shanghai Jiao Tong University, 800 Dong Chuan Road, Shanghai 200240, China
[b] Key Laboratory of Magnetic Materials and Devices, Ningbo Institute of Material Technology and Engineering, Chinese Academy of Sciences, Ningbo 315201, China
[c] Zhejiang Province Key Laboratory of Magnetic Materials and Application Technology, Ningbo Institute of Material Technology and Engineering, Chinese Academy of Sciences, Ningbo 315201, China

ARTICLE INFO

Article history:
Received 22 April 2015
Revised 25 May 2015
Accepted 25 May 2015
Available online 24 June 2015

Keywords:
Elastocaloric effect
Heusler alloys
Shape memory alloy
Martensitic transformation

ABSTRACT

The elastocaloric effect of the $[001]_P$ and $[111]_P$ orientated (subscript P represents the parent phase) $Ni_{50}Fe_{19}Ga_{27}Co_4$ (at.%) single crystals exhibiting first-order martensitic transformations have been studied at temperatures of 298–448 K under different compressive stresses. The adiabatic temperature change ΔT_{adi} shows a significant dependence on the crystal orientation. The temperature decrease caused by adiabatic removal of stress 300 MPa reaches to about 9–10 K in a temperature range 328–398 K for $[0\,0\,1]_P$ specimen and 3 K at temperature near A_f for $[1\,1\,1]_P$ one. The large elastocaloric effect is essentially attributed to the entropy change during the stress-induced martensitic transformation. The accumulated defect such as the $a/2\langle 1\,1\,2\rangle$ $L1_0$ type dislocation is the main reason for the attenuation of the elastocaloric effect in a fatigue test up to 3000 cycles. Large specific adiabatic temperature ($|\Delta T_{adi}/\Delta\sigma| \approx 35$ K/GPa), wide specific effective temperature window ($|\Delta T_{win}/\Delta\sigma| \approx 320$ K/GPa) and high coefficient of performance (COP ≈ 14) in a temperature range as wide as 50 K during the unloading process enable the $[001]_P$ orientated $Ni_{50}Fe_{19}Ga_{27}Co_4$ single crystal as a potential elastocaloric material.

© 2015 Acta Materialia Inc. Published by Elsevier Ltd. All rights reserved.

1. Introduction

Caloric materials exhibiting large reversible isothermal entropy change (ΔS_{iso}) or adiabatic temperature change (ΔT_{adi}) under a driving field (including magnetic, uniaxial or isotropic stress and electric fields) are the potential alternative materials to the greenhouse gases in the conventional refrigeration system [1]. Among them, the elastocaloric materials (whose caloric effects are driven by the uniaxial stress) have attracted increasing attention and been assessed as the most promising materials for the future non-vapor compression refrigeration system by US Department of Energy [2,3].

Most investigations in elastocaloric materials are focused on the shape memory alloys (SMAs) which exhibit first-order martensitic transformations (MTs) [4–7]. Large elastocaloric effect in these SMAs mainly originates from the considerable entropy change during stress-induced MT, $\Delta S^{\sigma}_{trans}$. According to the Clausius–Clapeyron equation, $\Delta S^{\sigma}_{trans}$ can be expressed as

$$\Delta S^{\sigma}_{trans} = -\Delta\varepsilon^{T}(d\sigma/dT) \quad (1)$$

where σ is the critical stress for inducing MT at a given temperature T and $\Delta\varepsilon^{T}$ is the transformation strain. From Eq. (1), we can find that $\Delta\varepsilon^{T}$ is a key point to determine the elastocaloric effect in SMAs. Generally speaking, $\Delta\varepsilon^{T}$ usually shows a strong dependence on the crystal orientation, especially for the SMA exhibiting a large elastic anisotropy (C_{44}/C') [8]. However, the influence of crystal orientation on elastocaloric effect has not been studied yet.

Ni–Fe–Ga-based SMAs are new type of Heusler alloys whose mechanical behaviors are greatly improved through replacing Mn element in the classical Ni–Mn–Ga ferromagnetic SMA [9]. The thermal-induced MTs in these SMAs have been systematically investigated, which undergo the typical first-order MTs from the body-centered cubic B2 or Heusler $L2_1$ structure (parent phase) to the non-modulated $L1_0$ or modulated five-, six-, seven-layered structures (martensite phase) [10,11]. The transformation temperatures can be controlled in a wide temperature range as wide as 160–400 K by substituting Co for Fe [12,13]. Meanwhile, several studies have focused on the stress-induced MTs in Ni–Fe–Ga-based SMAs. Large (~12%) and successive ($L2_1$–10M–14M–$L1_0$) superelastic behaviors were reported in a $Ni_{54}Ga_{27}Fe_{19}$ (at.%) single crystal [14]. Wide temperature window (300–900 K) for stress-induced MT has been observed in a $Ni_{49}Ga_{27}Fe_{18}Co_6$ (at.%) single crystal [15], making it become a promising

* Corresponding authors at: Key Laboratory of Magnetic Materials and Devices, Ningbo Institute of Material Technology and Engineering, Chinese Academy of Sciences, Ningbo 315201, China (J. Liu), State Key Lab of Metal Matrix, School of Materials Science and Engineering, Shanghai Jiao Tong University, Shanghai 20240, China (X. Jin).
E-mail addresses: liujian@nimte.ac.cn (J. Liu), jin@sjtu.edu.cn (X. Jin).

http://dx.doi.org/10.1016/j.actamat.2015.05.054
1359-6454/© 2015 Acta Materialia Inc. Published by Elsevier Ltd. All rights reserved.

high-temperature SMA. Recently, large elastocaloric effect in a $Ni_{54}Ga_{27}Fe_{19}$ polycrystalline alloy has been reported [16]. However, this effect has not been reported in Ni–Fe–Ga-based single crystals. As reported in a previous literature [17], the elastic anisotropy, C_{44}/C', for a $Ni_{51.5}Fe_{21.5}Ga_{27.0}$ (at.%) alloy is calculated to be 6.6, which is much higher than that of famous Ni–Ti SMA ($C_{44}/C' \approx 2$) [18]. This implies that, the elastocaloric effect in Ni–Fe–Ga-based single crystal is expected to exhibit a strong dependence on crystal orientation.

In addition, for the application of elastocaloric materials, an important factor is the stability of temperature change in its entire service life. A remarkably long fatigue life over exceeding 13,000 cycles at a 10% strain has been reported in a $[001]_P$ orientated $Ni_{54}Fe_{19}Ga_{27}$ (at.%) single crystal [19]. Therefore, it is necessary to evaluate the stability of elastocaloric effect of the Ni–Fe–Ga-based single crystals under a long-term fatigue test.

In this paper, we will systematically study the mechanical behavior and elastocaloric effect of the $Ni_{50}Fe_{19}Ga_{27}Co_4$ (at.%) single crystals with different crystal orientations. The origins of their elastocaloric effect will be explored. The stability of the elastocaloric effect will be investigated, by taking into account the defects created in a long-term stress-cycling test.

2. Experiments

Ingots of $Ni_{50}Fe_{19}Ga_{27}Co_4$ (at.%, in nominal composition) alloy were prepared by arc melting high purity metals of Ni (99.98%), Fe (99.99%), Ga (99.99%) and Co (99.98%) in argon atmosphere. Single crystals were grown by Bridgman technique in an inert gas atmosphere. The orientation of the crystal axis was determined in the parent phase by a high temperature back-reflection Laue camera. Two rectangular compressive specimens with the compressive axes along $[001]_P$ (3.9 mm $[100]_P \times 4.0$ mm $[010]_P \times 7.8$ mm $[001]_P$) and $[111]_P$ (4.0 mm $[1\bar{1}0]_P \times 4.0$ mm $[11\bar{2}]_P \times 8.7$ mm $[111]_P$) directions were cut by electro-discharge machining. In the present paper, the index of crystal orientation is expressed as $[uvw]_P$ based on the cubic parent structure. The crystal structures and lattice parameters of the $Ni_{50}Fe_{19}Ga_{27}Co_4$ alloy were determined by an *in situ* X-ray diffractometer (XRD) using copper K_α radiation. The parent phase was determined at 373 K as a cubic $L2_1$ structure with $a_0 = 0.576$ nm. The martensite structure was indentified as a non-modulated tetragonal $L1_0$ martensite structure at room temperature with the corresponding parameters $a = 0.763$ nm, $c = 0.656$ nm. These lattice parameters are in good agreement with those reported in previous studies [12,20].

The magnetic properties were analyzed using a superconducting quantum interference device (SQUID) magnetometer Quantum Design MPMS-5S. The martensitic transformation temperatures and latent heats were characterized by a differential scanning calorimeter (DSC) NETZSCH model 200F3, and the heat capacity was calibrated using a standard sapphire sample.

Compressive tests were conducted on a testing machine (Autograph AG-I 50 kN MODEL M1, Shimadzu) in a temperature range of 298–448 K. During the compressive tests, the specimen was mounted in a die and the stress was applied through a pair of pistons as illustrated in Fig. 1(a). The stress–strain curves at different temperatures were recorded at a strain rate of 2×10^{-3} s^{-1}. The strain was obtained by calibrating the crosshead displacement. The temperature changes under different compressive stresses at different temperatures were measured in a process as below. Firstly, the compressive stress was increased at a strain rate of 0.05 s^{-1} until reaching to exactly the set stress, and held for 30 s to make sure that the specimen temperature returned back to the original value. Then, unloading the stress at a strain rate of 0.13 s^{-1} to approximately the adiabatic condition; and finally, the zero-stress status was kept for 40 s.

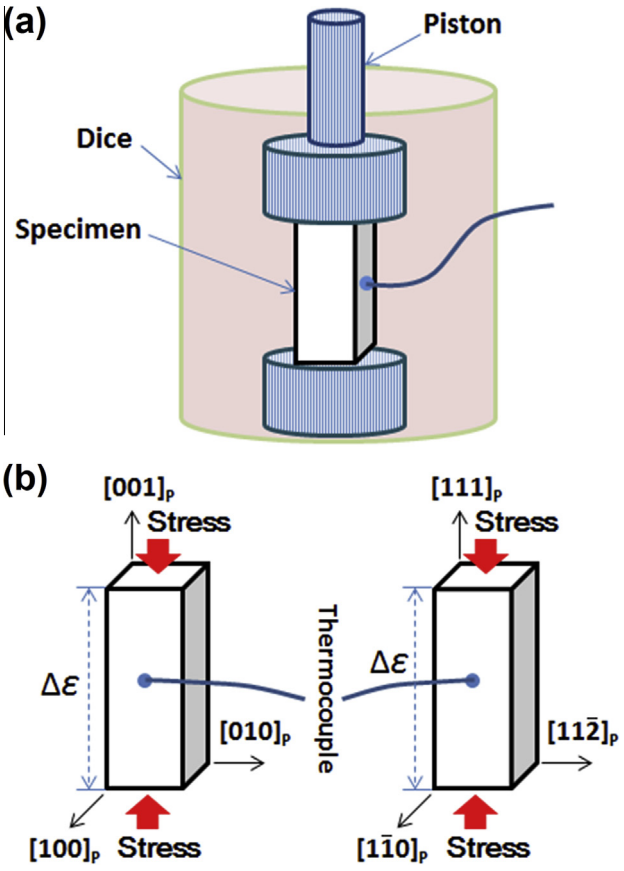

Fig. 1. A sketch of the experimental setup (a) and specimens (b) for mechanical tests.

In the long-term fatigue experiment, the compressive stress was applied at a strain rate of 0.09 s^{-1} and immediately removed at the same strain rate. It should be mentioned that, in the repeated cycling test, the actually applied stress could be slightly different from the set value due to the relatively high strain rate. The specimen temperature change induced by the stress change was monitored by a T-type thermocouple welded onto the center of specimen surface as illustrated in Fig. 1(b). During the cycling test, the thermocouple was welded to the specimen again after each 1000 cycles so as to avoid any loose contact between them.

Microstructure of the specimen was observed on a transmission electron microscope (TEM). The disks were spark cut from the specimens before and after fatigue test. They were then thinned by a Gatan Precision Ion Polishing system, Model 695. TEM observations were performed at room temperature using a JOEL 2100F at an accelerating voltage of 200 keV.

3. Results

3.1. Martensitic transformation behaviors

Fig. 2 shows the magnetic moment of the polycrystalline $Ni_{50}Fe_{19}Ga_{27}Co_4$ as a function of temperature in a weak magnetic field of 10 mT with cooling and heating rates of 3 K/min. Based on the strong magnetic anisotropy of martensite phase, the MT was detected by the sudden variations on the curves, of which the characteristic temperatures were determined through the extrapolated onset and offset temperatures as shown in Fig. 2.

Upon cooling, the ferromagnetic parent phase transforms into the ferromagnetic martensite phase; and the reverse MT occurs

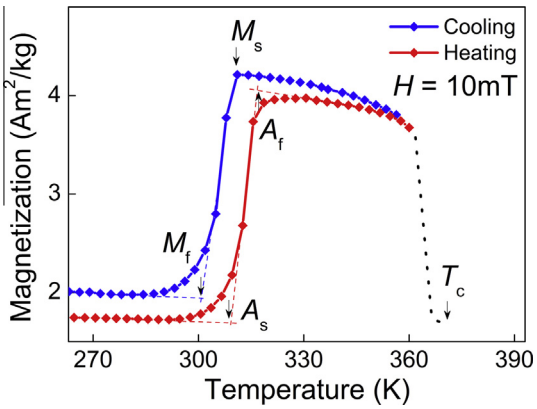

Fig. 2. Magnetization of the $Ni_{50}Fe_{19}Ga_{27}Co_4$ (at.%) polycrystal as a function of temperature under a magnetic field of 10 mT.

in the heating process. The Curie temperature was determined as that the magnetization suddenly drops to zero. These transformation temperatures are listed in Table 1.

The characteristic MTs were also detected by DSC measurement with cooling and heating rates of 10 K/min. Two small $[001]_P$ and $[111]_P$ orientated specimens were used and the results are presented in Fig. 3(a) and (b), respectively. The exothermic/endothermic peak appeared during cooling/heating process corresponds to the forward/reverse thermal-induced MT. The determined M_s, M_f, A_s and A_f are also listed in Table 1. The difference in M_s, M_f, etc., determined from $[001]_P$ and $[111]_P$ specimens might result from that in the composition of two ingots.

Through integrating the areas of peaks in Fig. 3(a) and (b), the latent heats Q^{For} and Q^{Rev}, where For and Rev stand for "forward" and "reverse" MTs, respectively, were estimated and the corresponding thermal-induced MT entropy change ΔS^T_{trans} can be evaluated by an expression as below:

$$\Delta S^T_{trans} = Q/T_0, \tag{2}$$

where T_0 is the equilibrium temperature defined as $(M_s + A_f)/2$ [21]. The calculated results are included in Table 1 as well. The calculated heat capacity C_p as a function of T under a constant pressure in the heating process are shown in Fig. 3(c) and (d). Since the peaks of C_p near 310 and 330 K in the curves are caused by the latent heats, the value of base line for C_p would be employed in the later calculations.

3.2. Microstructure of the martensite phase

Fig. 4(a) presents a TEM bright field image of martensite phase in $Ni_{50}Fe_{19}Ga_{27}Co_4$ alloy with Fig. 4(b) showing the selected area diffraction (SAD) pattern. The SAD pattern indicates a typical twin-related $L1_0$ martensite structures with the beam direction [110]. The thickness of twin plates is approximately 20–50 nm with {111} twin boundaries. In Fig. 4(b), the measured angle θ (about 101°) between $(2\bar{2}2)$ and $(\bar{2}22)$ reflections is consistent with that calculated from the $L1_0$ lattice parameters as presented in Section 2.

Table 1
Martensitic transformation temperatures (M_s, M_f, etc.), Curie temperature (T_C), latent heats (Q) and thermal-induced entropy change (ΔS^T_{trans}) of the polycrystalline, $[001]_P$ and $[111]_P$ orientated $Ni_{50}Fe_{19}Ga_{27}Co_4$ single crystals.

$Ni_{50}Fe_{19}Ga_{27}Co_4$	M_s (K)	M_f (K)	A_s (K)	A_f (K)	T_c (K)	Q^{For} (J/mol)	Q^{Rev} (J/mol)	ΔS^T_{trans} (For) (J/(mol K))	ΔS^T_{trans} (Rev) (J/(mol K))
Polycrystalline	310.9	300.4	308.9	317.5	370.3	–	–	–	–
Single crystal $[001]_P$	304.8	296.5	310.0	320.0	–	−290.9	280.0	−0.95	0.91
Single crystal $[111]_P$	302.6	297.8	324.3	328.9	–	−279.5	263.2	−0.89	0.84

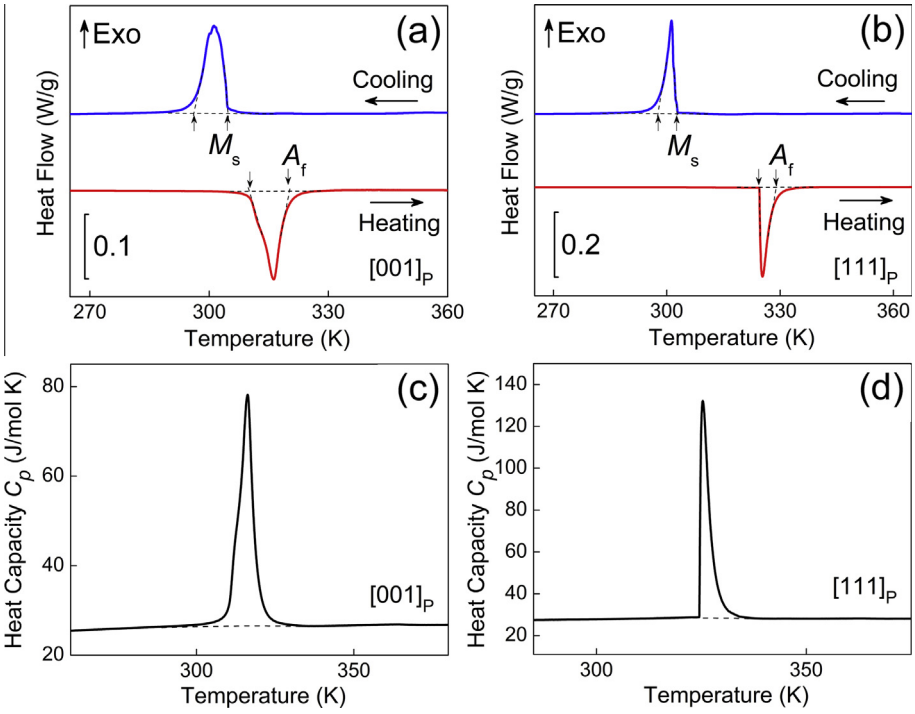

Fig. 3. Temperature dependence of the heat flow (a and b) and heat capacity C_p, (c and d) of the $[001]_P$ (a and c) and $[111]_P$ (b and d) orientated $Ni_{50}Fe_{19}Ga_{27}Co_4$ (at.%) single crystals.

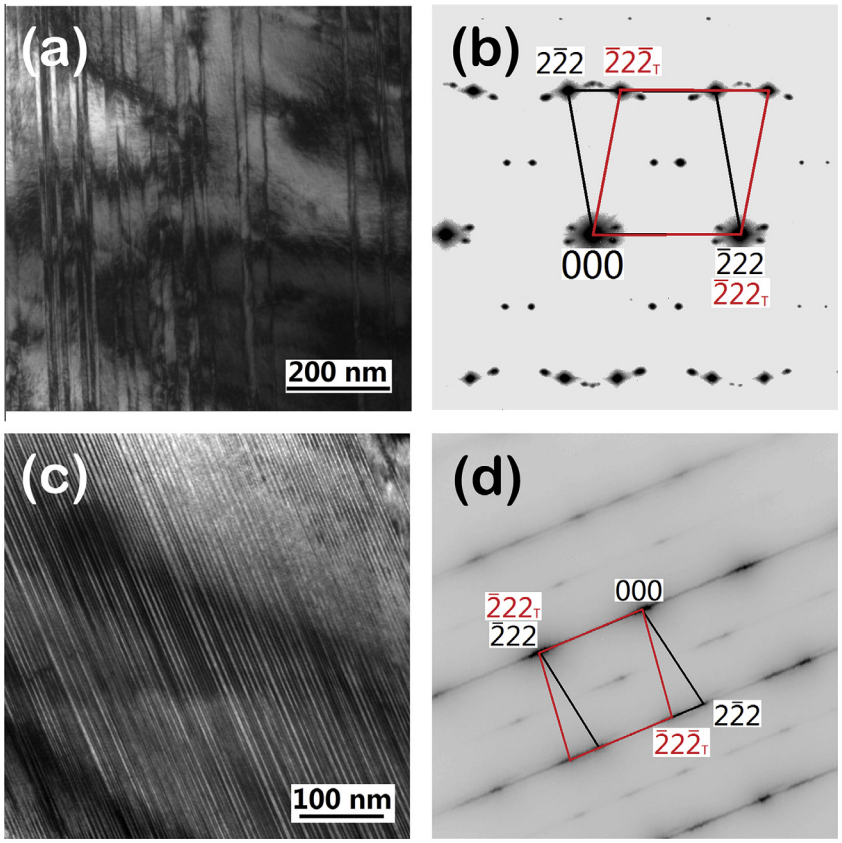

Fig. 4. Bright filed TEM micrographs (a and c) and the corresponding selected area diffraction patterns, showing two types of twinned martensitic structure, *i.e.*, the modulated (b) and very fine twins (d), in the $Ni_{50}Fe_{19}Ga_{27}Co_4$ (at.%) alloy.

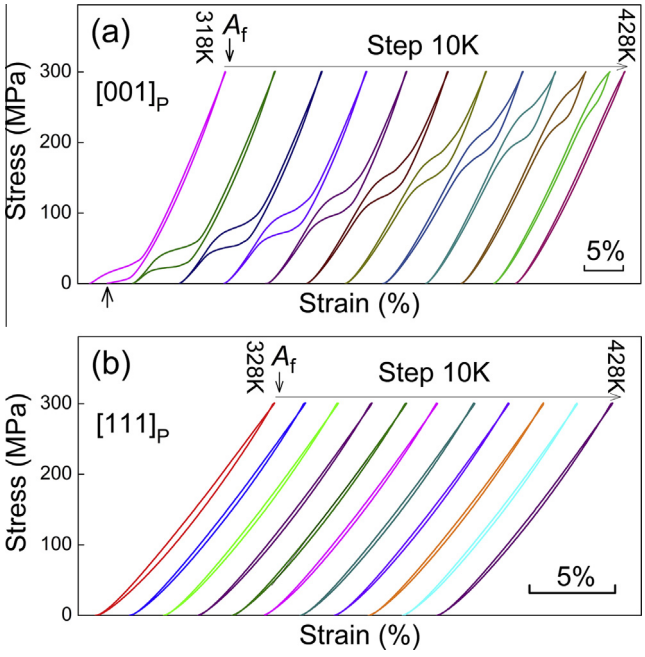

Fig. 5. Stress–strain curves of the $[001]_P$ (a) and $[111]_P$ (b) orientated $Ni_{50}Fe_{19}Ga_{27}Co_4$ (at.%) single crystals, up to a compressive stress of 300 MPa at various temperatures, stepped by 10 K between each other.

It is worthy to note that two sets of satellite reflections are visible around each fundamental Bragg spot. They are considered to be caused by the structural modulation, which was also reported in the Ni_2FeGa alloys [22,23]. However, the modulated structure was not detected by XRD measurement. This may be due to its too small volume fraction of modulated structure.

In addition, other much finer twin plates with the thickness of 4–7 nm were also observed, and a typical bright field image is shown in Fig. 4(c). Correspondingly, the SAD pattern in Fig. 4(d) contains diffuse streaks along $\langle\bar{2}22\rangle$ directions. These diffuse streaks are caused by very fine {1 1 1} twins and were also reported for the martensite phase of Ni–Mn–Ga alloy [24].

3.3. Mechanical behaviors

Fig. 5(a) shows the stress–strain curves of the $Ni_{50}Fe_{19}Ga_{27}Co_4$ single crystal compressed in $[001]_P$ direction up to a maximum stress of 300 MPa at various temperatures. In the present case, the stress and strain are with negative values. At 318 K, relatively flat "plateau" appeared in the stress–strain curves in both the loading and unloading processes, typically indicating the stress-induced MT. Note that a residual strain of −2.3%, as indicated by an arrow, is obtained after removing the stress. The reason is the coexistence of parent and martensite phases at 318 K (a little bit lower than A_f = 320.0 K for the present specimen), and the parent phase exhibits superelastic behavior. At the temperatures above A_f, the stress–strain curves indicate the complete superelastic behavior with a maximum recoverable strain close to 18%. Meanwhile, the "plateau" gradually moves to the higher stress with increasing temperature and disappears at above 428 K. This behavior will be further discussed in Section 4.1.

Compressive tests were also conducted on the $Ni_{50}Fe_{19}Ga_{27}Co_4$ single crystal with $[1\,1\,1]_P$ loading axis as shown in Fig. 5(b). In the testing region 328–428 K, the curves seem to be approximately linear with only small hysteresis and they reach almost the same

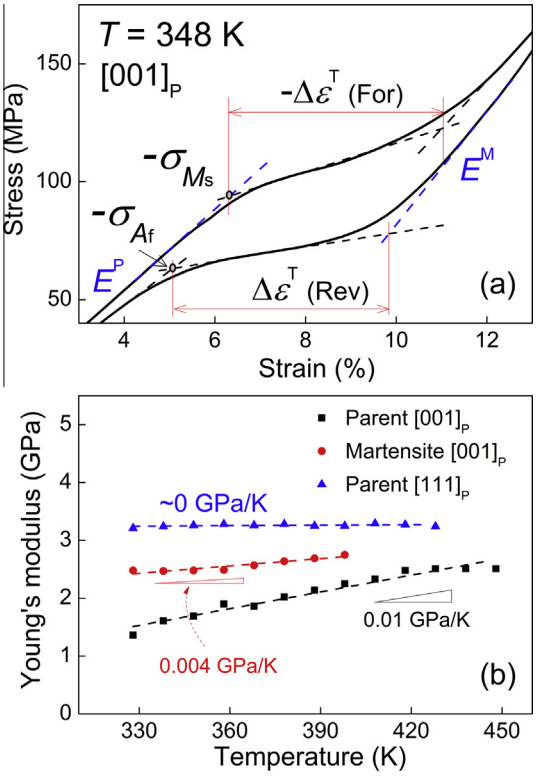

Fig. 6. (a) Schematic illustration showing the determination of Young's modulus for the parent (E^P) or martensite (E^M) phases, in which the transformation strains $\Delta\varepsilon^T$ (For)/(Rev) and critical stresses σ_{M_s}, σ_{A_f} for the $[001]_P$ orientated $Ni_{50}Fe_{19}Ga_{27}Co_4$ (at.%) single crystal at 348 K were taken as an example. (b) Temperature dependence of Young's modulus of the parent and martensite phases in the $[001]_P$ and $[111]_P$ directions for the $Ni_{50}Fe_{19}Ga_{27}Co_4$ (at.%) single crystals.

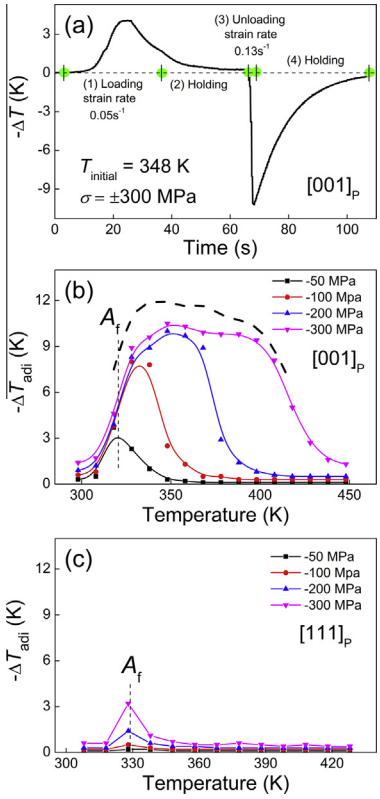

Fig. 7. (a) The experimental temperature change, ΔT, as a function of time for the $Ni_{50}Fe_{19}Ga_{27}Co_4$ (at.%) single crystal induced by a compressive stress of 300 MPa in the $[001]_P$ direction at 348 K. (b) Adiabatic temperature change $-\Delta T_{adi}$ for the $[001]_P$ (b) and $[111]_P$ (c) orientated $Ni_{50}Fe_{19}Ga_{27}Co_4$ (at.%) single crystals caused by the removal of compressive stress of 50 MPa, 100 MPa, 200 MPa and 300 MPa. The black dashed line in (b) is evaluated effect from the entropy change during the stress-induced MT.

maximum recoverable strain about 10%. The absence of "plateau" in the stress–strain curves for the $[111]_P$ orientated $Ni_{50}Fe_{19}Ga_{27}Co_4$ single crystal means that there could not be obvious stress-induced MT occurred upon compression.

Based on the stress–strain curves in Fig. 5, the Young's modulus in $[001]_P$ and $[111]_P$ directions of $Ni_{50}Fe_{19}Ga_{27}Co_4$ single crystals can be evaluated. As exemplified in Fig. 6(a) which is the enlarged part of the 348 K curve containing the "plateau" for $[001]_P$ specimen, the Young's modulus of the parent (E^P) or martensite (E^M) phases was determined from the steepest linear sections of curves as shown by the blue dashed lines. The measured temperature dependence of E^P and E^M are summarized in Fig. 6(b). It is found that the Young's modulus of $Ni_{50}Fe_{19}Ga_{27}Co_4$ single crystals is not sensitive to temperature. For $[001]_P$ orientated specimen, the slopes of E^P and E^M are only 0.01 GPa/K and 0.004 GPa/K, respectively and of E^P for $[111]_P$ specimen is almost zero.

3.4. Elastocaloric effect

Fig. 7(a) shows the temperature change ΔT of the $Ni_{50}Fe_{19}Ga_{27}Co_4$ single crystal compressed in the $[001]_P$ direction as a function of time at 348 K (furnace temperature). With increasing the compressive stress up to 300 MPa, the maximum temperature increase reached 4.1 K and decreased by 10.2 K happened when suddenly unloaded. Such a large temperature deviation between the loading and unloading processes is attributed to the large difference in their strain rates, *i.e.*, the strain rate in unloading process is over two times of that in the loading. Due to the quick stress removing, the measured ΔT in unloading (−10.2 K) can be reasonably recognized as the adiabatic change (ΔT_{adi}) under the given conditions.

Similarly, such measurements were also conducted at other temperatures and the maximum compressive stresses in a range of 50–300 MPa. The adiabatic temperature changes ($\Delta T_{adi} < 0$) in the unloading process are presented in Fig. 7(b). It is seen that under a compressive stress of 50 MPa, $-\Delta T_{adi}$ shows a peak at a temperature near A_f. With increasing the applied stress, the shape of $-\Delta T_{adi} \sim T$ curve gradually changes to a trapezium, which is the characteristic of elastocaloric effect for SMAs exhibiting typical first-order MT [4]. In the temperature range 328–398 K, $-\Delta T_{adi}$ reaches approximately 9–10 K under a compressive stress of 300 MPa.

Fig. 7(c) indicates the adiabatic temperature change of the $Ni_{50}Fe_{19}Ga_{27}Co_4$ single crystal compressed in the $[111]_P$ direction at different temperatures. It is noticed that an obvious $-\Delta T_{adi}$ of 3.2 K was only detected at temperature near A_f under a stress of 300 MPa and at the temperatures far away from A_f, $-\Delta T_{adi}$ becomes much less than 1 K.

3.5. Stability of elastocaloric effect

In order to assess the stability of elastocaloric effect in the $Ni_{50}Fe_{19}Ga_{27}Co_4$ single crystal, a long term mechanical cycling (up to 3000 times) test of the temperature change ΔT was conducted under a compressive stress of 300 MPa in $[001]_P$ loading axis at 348 K. ΔT at different stages in 1–5th, 1001–1005th, 1501–1505th and 2996–3000th cycles are compared in the same time scale as shown in Fig. 8(a). Maximum temperature change ΔT_{max} of each stage are indicated on the right side, and ΔT_{max} as a function of cycle number is re-plotted in Fig. 8(b) indicated by

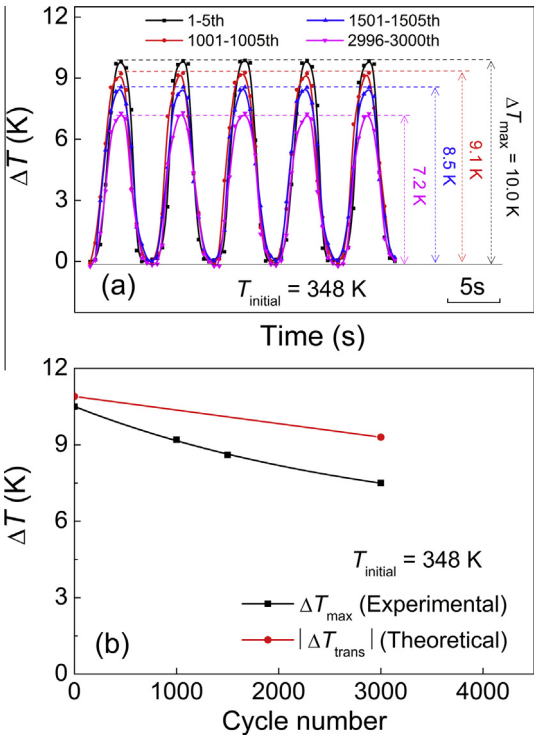

Fig. 8. (a) Temperature change, ΔT, as a function of time in the stages of 1–5th, 1001–1005th, 1501–1505th and 2996–3000th cycles for the $Ni_{50}Fe_{19}Ga_{27}Co_4$ (at.%) single crystal induced by a compressive stress of 300 MPa in the $[001]_P$ direction at 348 K. (b) Measured maximum temperature change ΔT_{max} (black curve) and theoretical transformation temperature change $|\Delta T_{trans}|$ (red line) as a function of cycle number. (For interpretation of the references to color in this figure legend, the reader is referred to the web version of this article.)

black points. It is found that ΔT_{max} decreases with increasing cycle number, but ΔT at each cycling stage keeps a similar profile. The temperature decreasing rate is calculated to be about 1×10^{-3} K/cycle where ΔT_{max} changes from 10.0 K (1–5th) to 7.2 K (2996–3000th). By using an exponential formula $\Delta T_{max} = A * \exp(-n/n_1) + B$ to fit the experimental data in Fig. 8(b), it is found that ΔT_{max} decreases to 5.7 K after an infinite number of cycles. The decrease of ΔT_{max} with increasing cycle number is mainly attributed to the accumulation of defects after long-term cycling, which will be further discussed in Section 4.2.

4. Discussion

4.1. The origin of the elastocaloric effect

The entropy change caused by the application and removal of an external stress for SMAs can include several parts as below:

$$\Delta S = \Delta S_{elec} + \Delta S_{mag} + \Delta S_{vib} \quad (3)$$

where ΔS_{elec}, ΔS_{mag} and ΔS_{vib} denote the entropy changes of electronic states, magnetic states and lattice vibration, respectively. Usually, ΔS_{elec} is negligibly small and is not taken into account. For the SMAs exhibiting large difference in the magnetization of parent and martensite phases, such as the Ni–Mn–In–Co metamagnetic system [25,26], ΔS_{mag} should be considered. However, due to the ferromagnetic property for both parent and martensite phases in the present $Ni_{50}Fe_{19}Ga_{27}Co_4$ alloy as shown in Fig. 2, ΔS_{mag} is also not to be considered. Then, large ΔS_{vib} can originate from the following two causes: (1) the lattice softening of parent or martensite phases during the elastic deformation and (2) the lattice displacive during the stress-induced MT. The first situation was confirmed in an Fe-31.2Pd (at.%) single crystal exhibiting a weak first-order MT, where the Young's modulus for the parent or martensite phases is significantly dependent on temperature [27,28]. However, Fig. 6(b) shows that the temperature dependence of the Young's modulus in both parent and martensite phases in present $Ni_{50}Fe_{19}Ga_{27}Co_4$ single crystals are quite small. Therefore, the entropy change mainly comes from the second cause, *i.e.*, the structural transformation. In the following, the temperature change ΔT_{trans} caused by the stress-induced MT will be calculated and compared with ΔT_{adi} obtained from the experiments.

For the $[001]_P$ orientated $Ni_{50}Fe_{19}Ga_{27}Co_4$ single crystal, the characteristics of stress-induced MT: such as the transformation strain $\Delta\varepsilon^T$ (For)/(Rev) upon loading/unloading process, the martensitic transformation starting stress σ_{M_s}, the martensitic transformation finishing stress σ_{A_f} are evaluated through an example in Fig. 6(a) at 348 K. Note that $\Delta\varepsilon^T$ (For), σ_{M_s} and σ_{A_f} are having negative values, and that of $\Delta\varepsilon^T$ (Rev) is positive. Based on the stress–strain curves in Fig. 5(a), the temperature dependence of $|\Delta\varepsilon^T|$ is presented in Fig. 9(a). It is found that $|\Delta\varepsilon^T|$ firstly increases in the temperature range 318–338 K with a maximum 4.8% and, then, gradually decreases with further increasing temperature. Incidentally, in the temperature range 398–418 K, the decreasing

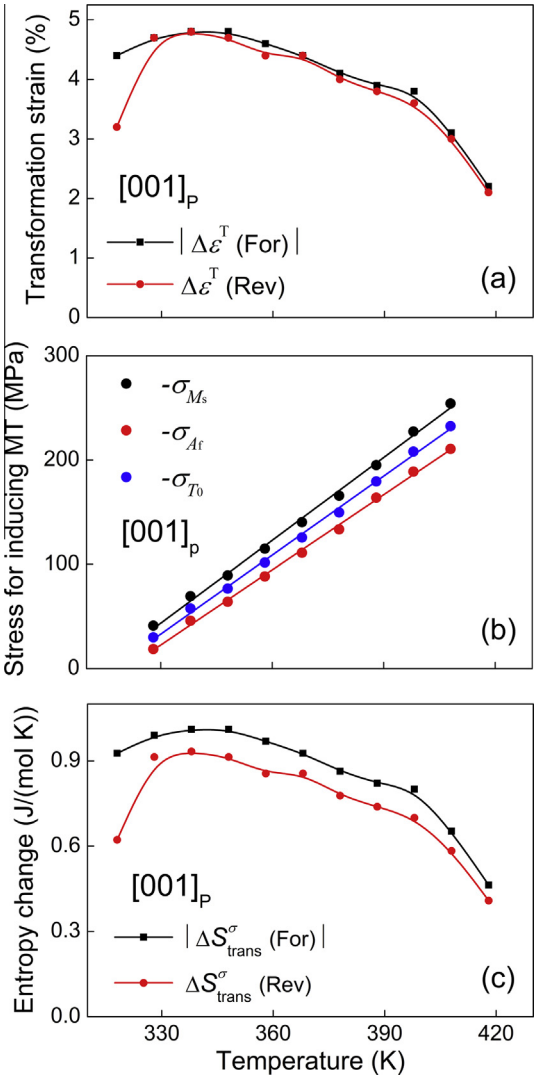

Fig. 9. Transformation strains $|\Delta\varepsilon^T|$ (a), critical stresses $-\sigma_{M_s}$, $-\sigma_{A_f}$ and $-\sigma_0$ (b) and entropy change caused by stress-induced MT $|\Delta S^{\sigma}_{trans}|$ (c) for the $[001]_P$ orientated $Ni_{50}Fe_{19}Ga_{27}Co_4$ (at.%) single crystal as function of temperature.

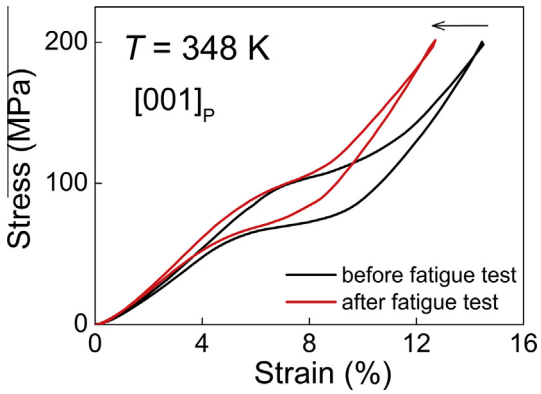

Fig. 10. Stress–strain curves before (black curve) and after (red curve) the fatigue test for the $[001]_P$ orientated $Ni_{50}Fe_{19}Ga_{27}Co_4$ (at.%) single crystal with a compressive stress of 200 MPa at 348 K. (For interpretation of the references to color in this figure legend, the reader is referred to the web version of this article.)

rate of $|\Delta\varepsilon^T|$ becomes more pronounced and was not observed above 428 K. The decrease of $|\Delta\varepsilon^T|$ in the temperature range 348–388 K can be partly attributed to a critical phenomenon where the first-order transformation is gradually changing to the second-order one. This behavior has been confirmed in a similar $Ni_{50}Fe_{19}Ga_{27}Co_4$ (at.%) single crystal [20] and also reported in an Fe-31.2Pd (at.%) single crystal [29]. However, the remarkable decrease of $|\Delta\varepsilon^T|$ in the temperature range 398–418 K should be mainly caused by the stress which is not sufficient to induce MT. This is especially correct for the disappearance of transformation strain at temperature above 428 K.

The critical stresses $-\sigma_{M_s}$, $-\sigma_{A_f}$ and the equilibrium stress $-\sigma_0$ $(=-(\sigma_{M_s}+\sigma_{A_f})/2)$ are indicated as a function of temperature in Fig. 9(b). Using a linear fitting, the slopes of $-\sigma_{M_s}$, $-\sigma_{A_f}$ and $-\sigma_0$ are determined to be 2.6 MPa/K, 2.4 MPa/K and 2.5 MPa/K, respectively. Then, from Eq. (1), $|\Delta S^{\sigma}_{trans}|$ at different temperatures was evaluated and the results are presented in Fig. 9(c). Note that $\Delta S^{\sigma}_{trans}$ (For) is negative in the loading process and $\Delta S^{\sigma}_{trans}$ (Rev) is positive in the unloading process. We find that, in the temperature range 328–368 K, $|\Delta S^{\sigma}_{trans}|$ reaches 0.89–0.97 J/(mol K) which is close to $|\Delta S^{T}_{trans}|$ obtained from the latent heat listed in Table 1. This means that the structural change for the $Ni_{50}Fe_{19}Ga_{27}Co_4$ single crystal under uniaxial $[001]_P$ stress may be same as that under thermal filed. However, the structure change under uniaxial stress in $[001]_P$ loading is not clear yet, and it will be a subject in the future.

The temperature change ΔT_{trans} caused by the entropy change during stress-induced MT can be approximately calculated through

$$\Delta T_{trans} \approx -\Delta S^{\sigma}_{trans} \cdot T/C \quad (4)$$

where C is the heat capacity under an uniaxial stress. Considering the small stress influence on C, we use the heat capacity under a constant pressure C_p in the present calculation as shown in Fig. 3(c). Then, we obtain $-\Delta T_{trans}$ (in the unloading process) as shown in Fig. 7(b) by a dashed curve. As expected, the calculated $-\Delta T_{trans}$ exhibits similar behavior with the experimentally obtained $-\Delta T_{adi}$ although these experimental values are lower than the calculated ones. The deviation would be mainly attributed to the insufficient adiabatic condition caused by the heat transfer to the piston and the surroundings air.

For the $[1\,1\,1]_P$ orientated $Ni_{50}Fe_{19}Ga_{27}Co_4$ single crystal, there is no obvious stress-induced MT observed in the loading and unloading processes. However, at temperature near A_f, a small extent of transformation may have occurred as confirmed by the adiabatic temperature change as shown in Fig. 7(c). This is also supported by a relatively large stress hysteresis at 328 K (close to A_f = 328.9 K for the present specimen). Due to the absence of "plateau" in the stress–strain curves, $-\Delta T_{trans}$ is indicated by the latent heat as listed in Table 1, and it was calculated to be 9.8 K. From Fig. 7(c), the maximum $-\Delta T_{adi}$ near A_f is only approximately one third of $-\Delta T_{trans}$ and becomes much smaller as the temperature is far away from A_f. However, whether there is any structural transformation under uniaxial $[1\,1\,1]_P$ stress needs further study.

4.2. Defects in the fatigue specimen

From Fig. 8, we know that the temperature change capability decreases with increasing cycle number. As the elastocaloric effect of the $Ni_{50}Fe_{19}Ga_{27}Co_4$ single crystal mainly comes from the entropy change during the stress-induced MT, the decrease of temperature change capability can be indicated by the decrease of transformation strain. Fig. 10 shows the stress–strain curves of the $[001]_P$ orientated $Ni_{50}Fe_{19}Ga_{27}Co_4$ single crystal under a compressive stress of 200 MPa before and after the fatigue test at 348 K. We note that $|\Delta\varepsilon^T|$ decreases approximately from 4.7% (1st) to 4% (3000th). According to the calculation mentioned in Section 4.1, $|\Delta T_{trans}|$ will change from 10.9 K to 9.3 K after 3000 cycles as indicated in Fig. 8(b) by a red line. It is found that the average decreasing rate for calculated $|\Delta T_{trans}|$ (6×10^{-4} K/cycle) is close to that of experimental ΔT_{max} (1×10^{-3} K/cycle).

The decrease of $|\Delta\varepsilon^T|$ means that the defects were accumulated when the interface between parent and martensite phases moved repeatedly. In order to observed the defects in the $[001]_P$ orientated $Ni_{50}Fe_{19}Ga_{27}Co_4$ single crystal, the specimen after 3000 times cycling test at 348 K was investigated by TEM at room temperature. Fig. 11(a) shows the dislocations in the twinned martensite

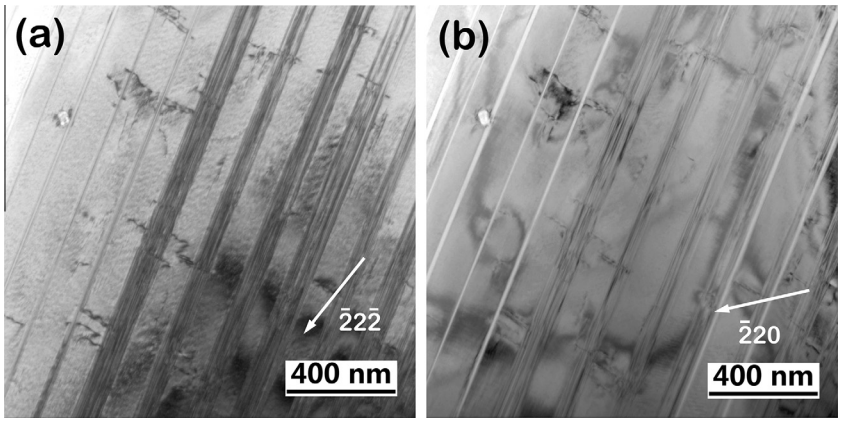

Fig. 11. The bright field TEM micrographs showing the dislocations within martensitic twins of the $[001]_P$ orientated $Ni_{50}Fe_{19}Ga_{27}Co_4$ (at.%) single crystal after 3000 times cycling test, by using the operating reflections $(\bar{2}2\bar{2})$ $L1_0$ (a) and $(\bar{2}20)$ $L1_0$ (b) reflections, respectively.

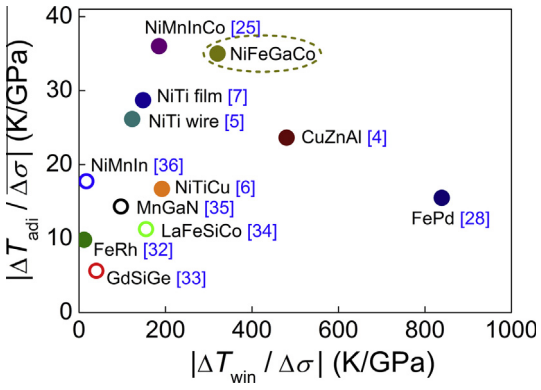

Fig. 12. A comparison of the specific adiabatic temperature change ($|\Delta T_{adi}/\Delta\sigma|$) and specific effective temperature window ($|\Delta T_{win}/\Delta\sigma|$) for various mechanocaloric materials including elastocaloric (solid cycles) and barocaloric (open cycles) ones. Except for the Ni–Fe–Ga–Co alloy, the data were taken from related literatures as quoted therein. The effective temperature windows for Ni–Ti-based SMAs are estimated from the critical stress–temperature phase diagram in Refs. [37,38].

with the operating reflection excited by $(\bar{2}\,2\,\bar{2})$ $L1_0$ reflection. Their Burgers vector was determined to be $a/2\langle 1\,1\,2\rangle$ $L1_0$ type by contrast analysis. The contrast obtained by exciting $(\bar{2}\,2\,0)$ $L1_0$ is shown in Fig. 11(b) as another example. $a/2\langle 1\,1\,2\rangle$ is the second shortest Burgers vector lying on {1 1 1} planes for $L1_0$ structure which was also reported in deformed TiAl alloy [30].

4.3. Compared with other mechanocaloric materials

For a caloric material, the adiabatic temperature change ΔT_{adi} and the effective temperature window ΔT_{win} are two important factors to determine the caloric effect. ΔT_{win} is defined as the temperature range where ΔS_{iso} or ΔT_{adi} is higher than a half of its maximum value [31]. On the other hand, for the mechanocaloric materials (including elastocaloric and barocaloric materials), the value of applied uniaxial or isotropic stress is necessary to be considered. The higher stress is employed, the more energy is required to induce the caloric effect. Therefore, in the following comparison, the specific caloric effects $|\Delta T_{adi}/\Delta\sigma|$ and $|\Delta T_{win}/\Delta\sigma|$ are taken into account. Such a comparison for a number of mechanocaloric materials [4–7,25,28,32–36] is shown in Fig. 12, where elastocaloric and barocaloric materials are indicated by solid and open circles, respectively. It is found that, the $[001]_P$ orientated $Ni_{50}Fe_{19}Ga_{27}Co_4$ single crystal shows a high level of caloric effect with a large $|\Delta T_{adi}/\Delta\sigma| \approx 35$ K/GPa and a wide $|\Delta T_{win}/\Delta\sigma| \approx 320$ K/GPa, which are both higher than those for famous Ni–Ti-based SMAs.

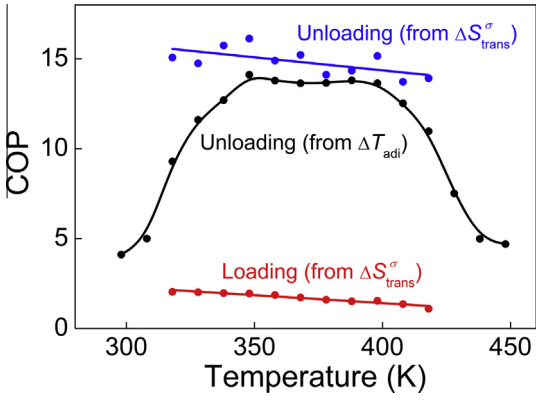

Fig. 13. The coefficient of performance (COP) for the $[001]_P$ orientated $Ni_{50}Fe_{19}Ga_{27}Co_4$ single crystal in the loading and unloading processes, deduced from different data as indicated.

On the other hand, the coefficient of performance (COP) is another important parameter of cooling technologies. According to Ref. [5], the COP is obtained by dividing the cooling power by input work. The cooling power can be estimated from $\Delta S^{\sigma}_{trans}$, where the entropy change $\Delta S^{\sigma}_{trans}$ is originated from Fig. 9(c), or from $\Delta T_{adi} \cdot C_p$, where ΔT_{adi} is obtained from Fig. 7(b). The input work in the loading process can be calculated by integrating the area enclosed by the stress–strain curve and the horizontal axis in Fig. 5(a), and that in the unloading process is evaluated from the area enclosed between the loading and the unloading curves. The calculated COPs for the $[001]_P$ orientated $Ni_{50}Fe_{19}Ga_{27}Co_4$ single crystal in the loading and unloading processes at different testing temperatures are presented in Fig. 13. It is found that, in the temperature range of 318–418 K, the COPs (from ΔT_{adi}) in the loading and unloading processes reach to about 1.7 and 15, respectively. Meanwhile, the COPs (from $\Delta S^{\sigma}_{trans}$) in the unloading process can reach to 14 in the temperature range of 348–398 K. It is worthy to note that the COP for the $[001]_P$ orientated $Ni_{50}Fe_{19}Ga_{27}Co_4$ single crystal in the unloading process, used for the elastocaloric cooling, is higher than that of Ni–Ti alloy (COP = 11.8 [5]). Through modifying Co-content, the MT temperatures of Ni–Fe–Ga–Co SMAs can span in a wide temperature range (over 200 K) [12,13]. In other words, it is easy to control the effective temperature window from low to high temperature ranges. In addition, the noble metal free, non-toxic element constitution and good oxidation resistance of $Ni_{50}Fe_{19}Ga_{27}Co_4$ alloy are other advantages for the application as a caloric material.

5. Conclusions

The elastocaloric effect of the $[001]_P$ and $[111]_P$ orientated $Ni_{50}Fe_{19}Ga_{27}Co_4$ (at.%) single crystals exhibiting the first-order MTs have been assessed in a temperature range 298–448 K under different compressive stresses. The following results were obtained.

1. The adiabatic temperature change ΔT_{adi} shows a strong dependence on the crystal orientation. The temperature decrease caused by the removal of adiabatic stress 300 MPa can reach to about 9–10 K in a temperature range 328–398 K for the $[001]_P$ orientated $Ni_{50}Fe_{19}Ga_{27}Co_4$ single crystal and 3 K at temperature near A_f for the $[111]_P$ orientated one.
2. The elastocaloric effect for the $[001]_P$ orientated $Ni_{50}Fe_{19}Ga_{27}Co_4$ single crystal mainly originates from the entropy change during the stress-induced MT. The adiabatic temperature change is directly proportional to transformation strain.
3. The temperature change capability for the $[001]_P$ orientated $Ni_{50}Fe_{19}Ga_{27}Co_4$ single crystal decreases with increasing mechanical cycling number, which is attributed to the accumulated defects such as the $a/2\langle 1\,1\,2\rangle$ $L1_0$ type dislocations.
4. The large specific adiabatic temperature ($|\Delta T_{adi}/\Delta\sigma| \approx 35$ K/GPa), wide specific effective temperature window ($|\Delta T_{win}/\Delta\sigma| \approx 320$ K/GPa) and high coefficient of performance (COP ≈ 14) in a temperature range as wide as 50 K during the unloading process enable the $[001]_P$ orientated $Ni_{50}Fe_{19}Ga_{27}Co_4$ single crystal being a nice elastocaloric material promisingly.

Acknowledgments

The authors would like to thank Profs. T. Fukuda and T. Kakeshida (Osaka University) for their valuable support. The authors would also like to thank Prof. S. Chen (Shanghai Jiao Tong University) for his careful reading. This work was funded by

the National Natural Science Foundation of China (51371184) and Zhejiang Provincial Natural Science Foundation (LR14E010001). This work was also sponsored by Shanghai Pujiang Program.

References

[1] X. Moya, S. Kar-Narayan, D. Mathur, Caloric materials near ferroic phase transitions, Nat. Mater. 13 (2014) 439, http://dx.doi.org/10.1038/NMAT3951.

[2] L. Mañosa, A. Planes, E. Vives, E. Bonnot, R. Romero, The use of shape-memory alloys for mechanical refrigeration, Funct. Mater. Lett. 2 (2009) 73, http://dx.doi.org/10.1142/S1793604709000594.

[3] W. Goetzler, R. Zogg, J. Young, C. Johnson, Energy Savings Potential and RDD Opportunities for Non-Vapor-Compression HVAC Technologies, prepared for U.S. Department of Energy, Navigant Consulting Inc, 2014.

[4] L. Mañosa, S. Jarque-Farnos, E. Vives, A. Planes, Large temperature span and giant refrigerant capacity in elastocaloric Cu–Zn–Al shape memory alloys, Appl. Phys. Lett. 103 (2013) 211904, http://dx.doi.org/10.1063/1.4832339.

[5] J. Cui, Y. Wu, J. Muehlbauer, Y. Hwang, R. Radermacher, Demonstration of high efficiency elastocaloric cooling with large ΔT using NiTi wires, Appl. Phys. Lett. 101 (2012) 073904, http://dx.doi.org/10.1063/1.4746257.

[6] C. Bechtold, C. Chluba, R. Lima de Miranda, E. Quandt, High cyclic stability of the elastocaloric effect in sputtered TiNiCu shape memory films, Appl. Phys. Lett. 101 (2012) 091903, http://dx.doi.org/10.1063/1.4748307.

[7] H. Ossmer, F. Lambrecht, M. Gültig, C. Chluba, E. Quandt, M. Kohl, Evolution of temperature profiles in TiNi films for elastocaloric cooling, Acta Mater. 81 (2014) 9, http://dx.doi.org/10.1016/j.actamat.2014.08.006.

[8] H. Horikawa, S. Ichinose, K. Morii, S. Miyazaki, K. Otsuka, Orientation dependence of $\beta_1 \rightarrow \beta_1'$ stress-induced martensitic transformation in a Cu–Al–Ni alloy, Metall. Trans. 19A (1988) 915, http://dx.doi.org/10.1007/BF02628376.

[9] K. Oikawa, Y. Imano, V.A. Chernenko, F.H. Luo, T. Omori, Y. Sutou, R. Kainuma, T. Kanomata, K. Ishida, Influence of Co addition on martensitic and magnetic transitions in Ni–Fe–Ga β based shape memory alloys, Mater. Trans. 46 (2005) 734, http://dx.doi.org/10.2320/matertrans.46.734.

[10] K. Oikawa, T. Ota, Y. Sutou, T. Ohmori, R. Kainuma, K. Ishida, Magnetic and martensitic phase transformations in a $Ni_{54}Ga_{27}Fe_{19}$ alloy, Mater. Trans. 43 (2002) 2360, http://dx.doi.org/10.2320/matertrans.43.2360.

[11] P.J. Brown, A.P. Gandy, K. Ishida, R. Kainuma, T. Kanomata, H. Morito, K.-U. Neumann, K. Oikawa, R.A. Ziebeck, Crystal structures and magnetization distributions in the field dependent ferromagnetic shape memory alloy $Ni_{54}Fe_{19}Ga_{27}$, J. Phys.: Condens. Matter 19 (2007) 016201, http://dx.doi.org/10.1088/0953-8984/19/1/016201.

[12] J. Liu, N. Scheerbaum, D. Hinz, O. Gutfleisch, Martensitic transformation and magnetic properties in Ni–Fe–Ga–Co magnetic shape memory alloys, Acta Mater. 57 (2008) 3177, http://dx.doi.org/10.1016/j.actamat.2008.03.008.

[13] H. Morito, K. Oikawa, A. Fujita, K. Fukamichi, K. Ishida, R. Kainuma, Control of phase transformation temperatures by substituents in Ni–Fe–Ga ferromagnetic shape memory alloys, Mater. Trans. 48 (2007) 2847, http://dx.doi.org/10.2320/matertrans.MI200714.

[14] Y. Sutou, N. Kamiya, T. Omori, R. Kainuma, K. Ishida, K. Oikawa, Stress–strain characteristics in Ni–Ga–Fe ferromagnetic shape memory alloys, Appl. Phys. Lett. 84 (2004) 1275, http://dx.doi.org/10.1063/1.1642277.

[15] E. Panchenko, Y. Chumlyakov, H.J. Maier, E. Timofeeva, I. Karaman, Tension/compression asymmetry of functional properties in [001]-oriented ferromagnetic NiFeGaCo single crystals, Intermetallics 18 (2010) 2458, http://dx.doi.org/10.1016/j.intermet.2010.09.009.

[16] Y. Xu, B. Lu, W. Sun, A. Yan, J. Liu, Large and reversible elastocaloric effect in dual-phase $Ni_{54}Fe_{19}Ga_{27}$ superelastic alloys, Appl. Phys. Lett. 106 (2015) 201903, http://dx.doi.org/10.1063/1.4921531.

[17] J.I. Pérez-Landazábal, V. Recarte, V. Sánchez-Alarcos, J.A. Rodríguez-Velamazán, M. Jiménez-Ruiz, P. Link, E. Cesari, Y.I. Chumlyakov, Lattice dynamics and external magnetic-field effects in Ni–Fe–Ga alloys, Phys. Rev. B 80 (2009) 144301, http://dx.doi.org/10.1103/PhysRevB.80.144301.

[18] X. Ren, N. Miura, J. Zhang, K. Otsuka, K. Tanaka, M. Koiwa, T. Suzuki, Y.I. Chumlyakov, M. Asai, A comparative study of elastic constants of Ti–Ni-based alloys prior to martensitic transformation, Mater. Sci. Eng. A-Struct. 312 (2001) 196, http://dx.doi.org/10.1016/S0921-5093(00)01876-1.

[19] C. Efstathiou, H. Sehitoglu, P. Kurath, S. Foletti, P. Davoli, Fatigue response of NiFeGa single crystals, Scr. Mater. 57 (2007) 409, http://dx.doi.org/10.1016/j.scriptamat.2007.04.049.

[20] A. Kosogora, V.A. L'vova, V.A. Chernenkoc, E. Villae, J.M. Barandiaranc, T. Fukuda, T. Terai, T. Kakeshita, Hysteretic and anhysteretic tensile stress–strain behavior of Ni–Fe(Co)–Ga single crystal: experiment and theory, Acta Mater. 66 (2014) 79, http://dx.doi.org/10.1016/j.actamat.2013.11.064.

[21] H.C. Tong, C.M. Wayman, Characteristic temperatures and other properties of thermoelastic martensites, Acta Metall. 22 (1974) 887, http://dx.doi.org/10.1016/0001-6160(74)90055-8.

[22] J.Q. Li, Z.H. Liu, H.C. Yu, M. Zhang, Y.Q. Zhou, G.H. Wu, Martensitic transition and structural modulations in the Heusler alloy Ni_2FeGa, Solid State Commun. 126 (2003) 323, http://dx.doi.org/10.1016/S0038-1098(03)00144-3.

[23] Z.W. Du, B.L. Shao, A.S. Liu, G.H. Wu, J.F. Qian, Z.Y. Zhang, Z. Gao, Martensitic transition and structural modulations in $Ni_{51}Fe_{24}Ga_{25}$ ferromagnetic shape-memory alloy, J. Mater. Sci. 46 (2011) 2733, http://dx.doi.org/10.1007/s10853-010-5146-4.

[24] J. Pons, V.A. Chernenko, R. Santamarta, E. Cesari, Crystal structure of martensitic phases in Ni–Mn–Ga shape memory alloys, Acta Mater. 48 (2000) 3027, http://dx.doi.org/10.1016/S1359-6454(00)00130-0.

[25] B. Lu, F. Xiao, A. Yan, J. Liu, Elastocaloric effect in a textured polycrystalline Ni–Mn–In–Co metamagnetic shape memory alloy, Appl. Phys. Lett. 105 (2014) 161905, http://dx.doi.org/10.1063/1.4899147.

[26] J. Liu, T. Gottschall, K.P. Skokov, J.D. Moore, O. Gutfleisch, Giant magnetocaloric effect driven by structural transitions, Nat. Mater. 11 (2012) 620, http://dx.doi.org/10.1038/NMAT3334.

[27] F. Xiao, T. Fukuda, T. Kakeshita, Significant elastocaloric effect in a Fe-31.2Pd (at.%) single crystal, Appl. Phys. Lett. 102 (2013) 161914, http://dx.doi.org/10.1063/1.4803168.

[28] F. Xiao, T. Fukuda, T. Kakeshita, X. Jin, Elastocaloric effect by a weak first-order transformation associated with lattice softening in an Fe-31.2Pd (at.%) alloy, Acta Mater. 87 (2015) 8, http://dx.doi.org/10.1016/j.actamat.2015.01.004.

[29] F. Xiao, T. Fukuda, T. Kakeshita, Critical point of martensitic transformation under stress in an Fe-31.2Pd (at.%) shape memory alloy, Phil. Mag. 95 (2015) 1390, http://dx.doi.org/10.1080/14786435.2015.1029561.

[30] G. Hug, A. Loiseau, A. Lasalmonie, Nature and dissociation of the dislocations in TiAl deformed at room temperature, Phil. Mag. A. 54 (1) (1986) 47, http://dx.doi.org/10.1080/01418618608242882.

[31] K.A. Gschneidner Jr., V.K. Pecharsky, A.O. Tsokol, Recent developments in magnetocaloric materials, Rep. Prog. Phys. 68 (2005) 1479, http://dx.doi.org/10.1088/0034-4885/68/6/R04.

[32] M.O. Annaorazov, S.A. Nikitin, A.L. Tyurin, K.A. Asatryan, A.Kh. Dovletov, Anomalously high entropy change in FeRh alloy, J. Appl. Phys. 79 (1996) 1689, http://dx.doi.org/10.1063/1.360955.

[33] S. Yuce, M. Barrio, B. Emre, E. Stern-Taulats, A. Planes, J. Tamarit, Y. Mudryk, K.A. Gschneidner Jr., V.K. Pecharsky, L. Mañosa, Barocaloric effect in the magnetocaloric prototype $Gd_5Si_2Ge_2$, Appl. Phys. Lett. 101 (2012) 071906, http://dx.doi.org/10.1063/1.4745920.

[34] L. Mañosa, D. González-Alonso, A. Planes, M. Barrio, J. Tamarit, I.S. Titov, M. Acet, A. Bhattacharyya, S. Majumdar, Inverse barocaloric effect in the giant magnetocaloric La–Fe–Si–Co compound, Nat. Commun. 2 (2011) 595, http://dx.doi.org/10.1038/ncomms1606.

[35] D. Matsunami, A. Fujita, K. Takenaka, M. Kano, Giant barocaloric effect enhanced by the frustration of the antiferromagnetic phase in Mn_3GaN, Nat. Mater. 14 (2015) 73, http://dx.doi.org/10.1038/NMAT4117.

[36] L. Mañosa, D. González-Alonso, A. Planes, E. Bonnot, M. Barrio, J.-L. Tamarit, S. Aksoy, M. Acet, Giant solid-state barocaloric effect in the Ni–Mn–In magnetic shape-memory alloy, Nat. Mater. 9 (2010) 478, http://dx.doi.org/10.1038/NMAT2731.

[37] S. Miyazaki, K. Otsuka, Y. Suzuki, Transformation pseudoelasticity and deformation behavior in a Ti-50.6at.%Ni alloy, Scripta, Metallalurgy 15 (1981) 287.

[38] F.J. Cil, J.A. Planell, Thermal efficiencies of NiTiCu shape memory alloys, Thermochim. Acta 327 (1999) 151, http://dx.doi.org/10.1016/S0040-6031(98)00607-8.